INTERNATIONAL JOURNAL OF NANO SCIENCE, NANO ENGINEERING AND NANOTECHNOLOGY
© Research Science Press
VOLUME 4 • NUMBER 1 • JANUARY-JUNE 2012 • ISSN : 2229-7383

The Growth of One-Dimensional Oxide Nanostructures by Thermal Oxidation of Metals

Lu Yuan[1], and Guangwen Zhou[2]*

ABSTRACT

The growth of one-dimensional oxide nanostructures by direct oxidation of metals has received extensive attention for its technical simplicity and large growth capabilities. However, the understanding of the basic mechanism leading to the spontaneous oxide whisker formation still remains essentially incomplete. Here we present a review of our systematic studies on the oxide nanowire growth from the oxidation of model metal systems, Cu and Fe. We show that the compressive stresses generated by the volume change associated with the interfacial reaction accompanying the layered oxide growth stimulate oxide nanowire formation and the one-dimensional oxide growth kinetics is controlled by surface diffusion of cations supplied by outward grain boundary diffusion through the oxide layers. We show that the oxide nanowire formation can be effectively promoted by surface bending tensile stress or surface roughening via sandblasting. We further demonstrate that oxygen gas pressure can be employed to manipulate the interfacial reaction, thereby allowing for tuning the oxide growth morphologies via the stress-driven grain boundary diffusion.

Keywords: *Oxidation, Cu, Fe, CuO, α-Fe2O3, Nanowire, stress, grain boundary*

1. INTRODUCTION

One-dimensional (1D) oxide nanostructures have been of broad interest from both the fundamental and applied aspects owning to potential wide technological applications of these nanomaterials. These 1D nanostructures find numerous applications in fields ranging from heterogeneous catalysis, energy conversion and storage, and environmental sensors to medical devices. The diversity of these applications is attributed to the unique advantages of oxides including high temperature stability, stable electronic and chemical properties and high oxidation resistance [1, 2]. Compared to other forms of oxide nanostructures, 1D metal oxide nanostructures have several advantages such as very large surface-to-volume ration, superior stability owing to the high crystallinity, possible surface functionalization, and the possibility of field-effect transistor configuration. In addition, the relatively simple preparation methods that allow large-scale production of 1D oxide nanostrucutres makes this form of nanostructures more attractive [1, 3, 4].

[1,2] Department of Mechanical Engineering & Multidisciplinary Program in Materials Science and Engineering, State University of New York, Binghamton, NY 13902

* Corresponding Author: *E-mail: gzhou@binghamton.edu*

Various approaches have been employed to generate 1D oxide nanosturctures, such as vapor-liquid-solid growth [5], vapor-solid growth [6], epitaxial growth [7], wet chemical methods [8], and electrospining [9]. The vapor-liquid-solid (VLS) growth involves three phases: the vapor phase precursor, the liquid catalyst droplet, and the solid crystalline product. The VLS mechanism contains the preparation of a catalytic liquid alloy droplet upon the substrate which can rapidly adsorb a vapor to supersaturation level, and from which crystal growth can subsequently occur. Wires grow only in the areas activated by the metal catalysts and the physical characteristics of nanowires (NWs) depend upon the size and physical properties of the liquid alloy. For instance, Seu Yi Li et al synthesized the ZnO NWs on copper coated p-type Si (1 0 0) substrate using VLS growth process, where Cu served as the catalyst for the 1D growth of ZnO NWs [10]. Using molten gallium as the catalyst, silicon oxide NWs tended to assemble into various complex morphologies through a metal-catalyzed VLS growth process [11]. SnO_2- NWs can also be synthesized by Au-catalytic oxidation of tin sputtered thin films [12].

The vapor-solid (VS) growth takes place when the NW crystallization originates from the direct condensation from the vapor phase without the use of a catalyst. Under high temperature condition, the source materials are vaporized and then directly condensed on the substrate in the low temperature region. The initially condensed molecules form seed crystals which serve as the nucleation sites for further condensation [1]. For example, single-crystalline NWs of indium oxide can be produced under controlled conditions via thermal evaporation of pure In_2O_3 powders and it was found that the seeding layer of the substrate was effective in promoting the NW nucleation [13]. Other kind of oxides, such as ZnO, has also been synthesized by single-step thermal evaporation method. There was no need of either any metal catalysts or a ZnO seed layer to synthesize the ZnO [14]. Y. Wang et al. prepared large-scale micro/nanosized Ga_2O_3 structures via a simple vapor phase growth method. The morphology of the as-grown structures depends strongly on its position and the growth temperature [15].

Epitaxial growth means a film grown on top of the crystalline substrate in preferred orientations that atomic arrangement of the film accepts crystallographic structure of the substrate. It contains molecular-beam epitaxy (MBE), solid-phase epitaxy, and liquid-phase epitaxy. It was shown that ZnO nanorods grown by site-selective molecular beam epitaxy show current-voltage characteristics that were sensitive to the presence of hydrogen or ozone [16]. It was reported that the GaN NWs grown by MBE on Al_2O_3 layer show a crystalline structure even at amorphous Al_2O_3 layer and the NWs are free of dislocations at the Al_2O_3 interface [17]. Wet chemical methods usually involve a solution-based catalyzed growth, which can be grouped into template-assisted and template-free methods. In this growth process, a nanoscale metallic droplet catalyzes the precursor decomposition and the crystalline NW growth, which is similar to the VLS method. Tapered, conical-shaped nanotubes were obtained by anodizing titanium foil in a 0.5% hydrofluoric acid electrolyte [18]. The synthesis of Cu_2O NWs is achieved by the reduction of cupric acetate with o-anisidine, pyrrole,

or 2, 5-dimethoxyaniline under hydrothermal conditions [19]. The electro spinning uses an electrical charge to draw very fine fibers with a diameter ranging from several micrometers to tens of nanometers from a liquid. Thus a sufficiently high voltage is needed to charge the liquid. This method is usually used for the production of polymeric nanofiber materials. The morphology of the fibers depends on the process parameters; including solution concentration, applied electric field strength, deposition distance and deposition time [9, 20]. As an example, the synthesis of polycrystalline ZnO nanowires was achieved by electro spinning method and the NWs were used in gas sensors for the detection of ethanol at 220°C [21]. Another example is tungsten oxide nanofibers grown by electrospinning. The large-scale WO_3 nanofibers have orthorhombic structure with diameter between 100 and 500 nm [22]. Some other oxides, such as Al_2O_3 and NiO, have also been fabricated by electro spinning method [23, 24].

Compared to these methods involving relatively complex and multi-step synthesis procedures as described above, oxide NW formation by direct thermal oxidation of metals is a simple approach with large-scale growth capabilities and has recently received intensive interest. Oxide whisker formation by oxidation of metals is a long-established phenomenon dating back to the 1950s [25]. Since then, numerous observations have been performed about the spontaneous oxide NW formation during the thermal oxidation of metals, however, the growth mechanism governing the 1D oxide growth has been widely debated and lacks cohesive understanding [26, 27]. Several mechanisms have been invoked to account for the oxidation induced 1D oxide NW growth as schematically shown in Fig. 1: (i) evaporation and condensation [28, 29], (ii) fast internal diffusion along a tunnel centered on the core of a screw dislocation [30, 31], and (iii) surface diffusion along the sides of NWs [32]. In mechanism (i), vapor-liquid-solid (VLS) [33] and vapor-solid (VS) [29, 34] have been most commonly used to explain the growth of NWs in the gas phase.

In VLS growth process, there is a catalyst (metal droplet) at the tip of the NWs, and the diameter of the NWs determined by the size of the metal droplet are uniform from bottom to top [35]. Based on the electron microscopy observations, it is known that no droplet occurs on the tip of oxide NWs, and the diameter of NWs reduces sharply at the tip range. Therefore, the VLS mechanism can be generally excluded. In VS process, the key step is evaporation of the oxide precursors at high temperatures followed by condensing at low temperature. This mechanism is not operative for oxide NW growth for obvious reasons of the requirement for the formation of highly volatile species, which usually does not occur at the intermediate oxidation temperatures. For instance, the melting points of Cu, Cu_2O, and CuO are 1085°C, 1243°C, and 1326°C, respectively [34, 36]. However, the oxidation temperature required for CuO NW growth during the thermal oxidation of Cu ranges from ~ 300°C to 600°C, far below the evaporating temperatures.

Some unique experiments have been performed and suggested that oxide NWs grow from the tip and are not extruded from the base oxide layers during the oxidation of Cu substrates [37, 38]. For such a process, the NW growth must call for transport of cation ions from the base to growth tip. It was suggested that oxide NWs or whiskers

grow predominately by surface diffusion of metal species from the NW base to tip along a tunnel centered on the core of a screw dislocation, as shown in Fig. 1(b) [37, 39-41]. However, such a scenario contradicts with many recent experimental observations, which reveal that oxide NWs have a bicrystal or single crystal structure (i.e., no hollow pipe present along the axial core of NWs) [26, 38, 42-44]. Therefore, it is paramount to identify the driving force leading to the initiation of oxide NW formation and the mass transport mechanisms governing the 1D oxide growth.

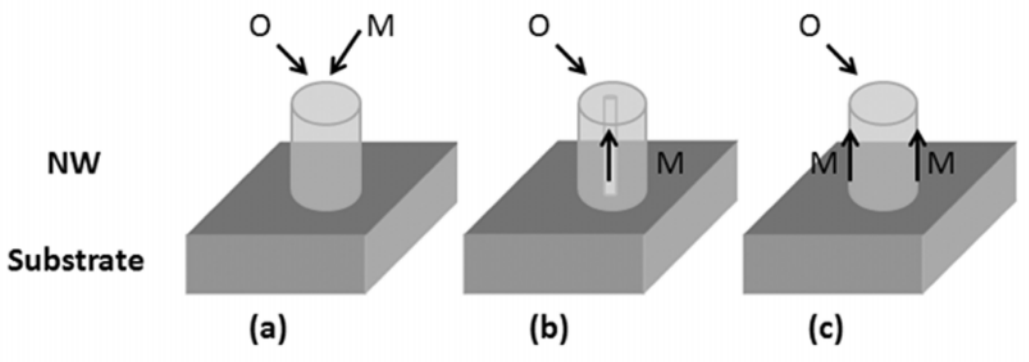

Figure 1: Comparison of the Various Mechanisms Proposed for Oxide NW Growth During the Oxidation of Metals: (a) Evaporation and Condensation; (b) Internal Diffusion Along the Core of a Screw Dislocation; (c) Surface Diffusion Along the Sidewall of a NW [67]

The phenomenon of oxide NW formation from the oxidation of metals is not tied up with a single metal system but the oxidation of Cu and Fe remains the most representative ones [45, 46]. The oxidation of Cu and Fe results in the growth of CuO NWs and α-Fe_2O_3 NWs, respectively. We choose Cu and Fe as the two model systems to understand the mechanism of oxidation-induced oxide NW growth. Meanwhile, our interest in these systems also stems from the prospective broad applications of nanostructured CuO and α-Fe_2O_3. A number of interesting properties have been found in these oxide materials that have led to its myriad technological applications in important fields. For instance, CuO is a p-type semiconductor with a narrow band gap of 1.2 eV, which has potential applications in many fields such as field emission, high temperature superconductors, heterogeneous catalysts, photovoltaic materials, and magnetic storage media [47, 48]. Hematite (α-Fe_2O_3) is an n-type semiconductor with a band gap of 2.1 eV, and has high stability under ambient conditions and low toxicity [49]. It can be used as a photoelectrode for solar energy conversion [50], gas sensor [51], heterogeneous catalysts [52], and magnetic recording media [53].

2. EXPERIMENTAL DETAILS

High-purity Cu and Fe foils (99.99% purity) are used in our study. For the oxidation of Cu, Cu foils are first cleaned in aqueous 1.0 M HCl solution to remove the native oxide layer and then thoroughly rinsed with deionized water followed by ultrasonication in acetone for 5 min. Fe foils are cleaned by thoroughly rinsing with deionized water followed by ultrasonication in acetone for 5 min. The cleaned metal

foils are then put on a substrate heater in a vacuum chamber, where the base pressure is ~2 10^{-6} Torr and the sample temperature is monitored using a K-type thermocouple in contact with the sample heater. The chamber is first pumped to vacuum (~2 10^{-6} Torr), and then filled with oxygen gas (the purity of oxygen is 99.999%). The chamber is then sealed and the annealed metal samples are heated to the desired temperature ranging from 300°C to 700°C at 20°C/min in the oxygen gas under the controlled gas pressure (pO_2). After the sample is oxidized for different durations (from 30 min to 4h), it is cooled down in the same oxygen atmosphere to room temperature at the rate of ~ 10°C/min. Surface morphology and chemical composition of the oxidized samples are examined using a field emission scanning electron microscope (FEG-SEM) FEI Supra 55VP. Length and diameter of nanowires are measured from SEM images. The morphology and microstructure of individual NWs are analyzed by transmission electron microscopy (TEM) using a JEOL 2100F operated at 200 kV.

3. CUO NW FORMATION BY OXIDATION OF CU

3.1. The Oxidation of Stress-Free Cu Surfaces

To study the growth mechanism of CuO NWs, we first examine the oxidation of stress-free Cu surface (i.e., flat Cu foils). Fig. 2a shows the typical surface morphology of CuO NWs on a Cu substrate oxidized at 450°C and pO_2 = 200 Torr for 1h. It can be seen that the surface is covered by dense CuO NWs, with diameters ranging from 50 to 100 nm and lengths up to several microns. The inset image in Fig. 2a shows a single CuO NW, which has smooth surface and uniform diameter along their longitudinal axial direction. Fig. 2b is a cross-sectional SEM image of an oxidized Cu sample, from which a three-layered structure can be indentified: a ~ 4 μm thick bottom Cu_2O layer lies directly above the Cu substrate, an intermediate CuO thin layer with a thickness of about 800 nm, and a top CuO NW layer relatively aligns perpendicular to the substrate surface. The Cu_2O layer shows detached from the Cu substrate because of the growth stress generated during the oxidation process.

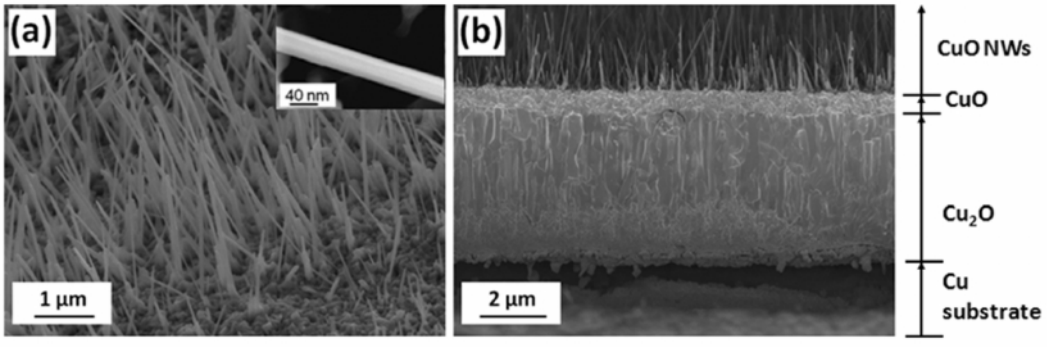

Figure 2: (a) The Surface Morphology of a Cu Substrate Oxidized at 450°C for 1h. Inset: Magnified SEM View of a Single CuO NW. (b) Cross-Sectional SEM Images Showing the CuO and Cu_2O layers on Cu Substrates

Figure 3 is an SEM image showing the initial growth stages of CuO nanowires. It can be seen that the oxide surface consists of highly faceted CuO grains and NWs are formed directly on top of grains. The oxide layer on the grain boundary regions hardly shows any signatures of formation of NWs. An instructive comparison comes from the occurrence of tin whisker growth on tin plated Cu lead frames, where the cross-sectional shape of Sn whiskers extruded from grain boundaries and whiskers show correlation with the grain boundary geometry at the surface [54]. As revealed in Fig. 3, the cross-sectional shapes of CuO NWs show no any correlation with the grain boundary geometry, suggesting that the oxide NW formation is not driven by a grain boundary extrusion process.

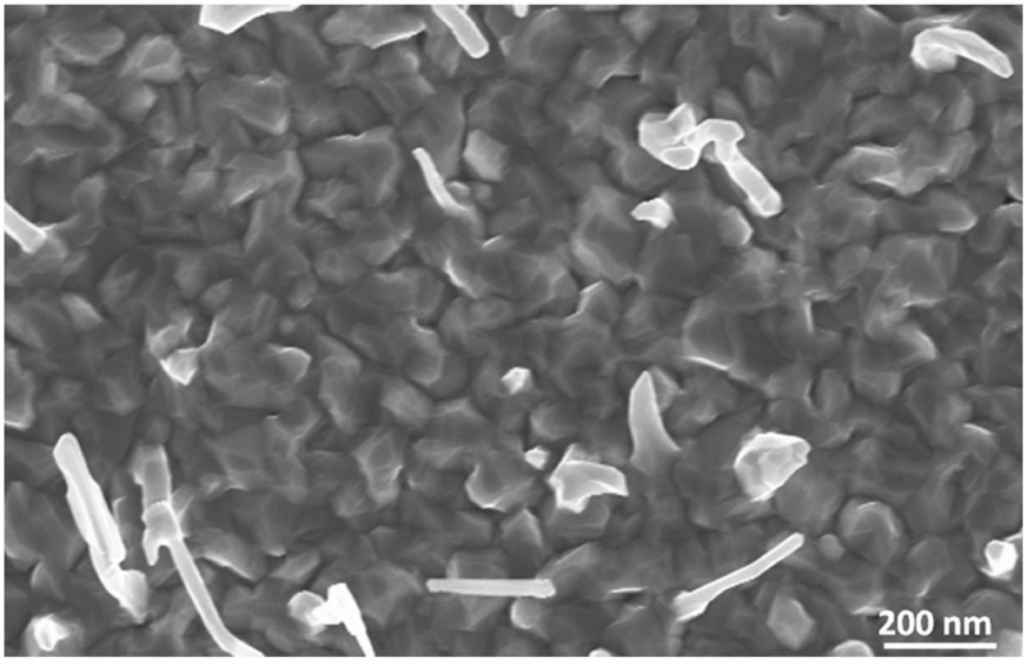

Figure 3: SEM micrograph of a Cu Substrate oxidized at 450°C for ~ 30 min, Showing the Initial Growth Morphology of CuO NWs [55]

Figure 4a displays a typical bright-field (BF) TEM image of an individual CuO NW synthesized by thermal oxidation, which reveals clearly that the NW is divided by a twin boundary along its length direction. Fig. 4b displays a high-resolution TEM (HRTEM) image, which shows that the NW has a bicrystalline structure and there is no hollow pipe along the core of the NW. Each side of the NW is single crystal with well-defined crystal lattice planes. The interplanar spacings of each side as measured from the HRTEM image are 2.52Å and 2.32Å, respectively, which are consistent well with the calculated lattice spacings of $(\bar{1}11)$ and $(\bar{1}11)$ planes of monoclinic CuO (a =4.69 Å, b=3.42 Å, c = 5.13 Å, and $\beta = 99.55^{o}$). A pertinent question is how

bicrystal (or twin) boundaries are generated in the NWs. As revealed from SEM observation, CuO grains are highly faceted and each facet would serve as a template for NW growth. The crystals grown on different facets are naturally joined together to form a twin or multi-twin structure started from the NW root and continued into the NW along the length direction [55].

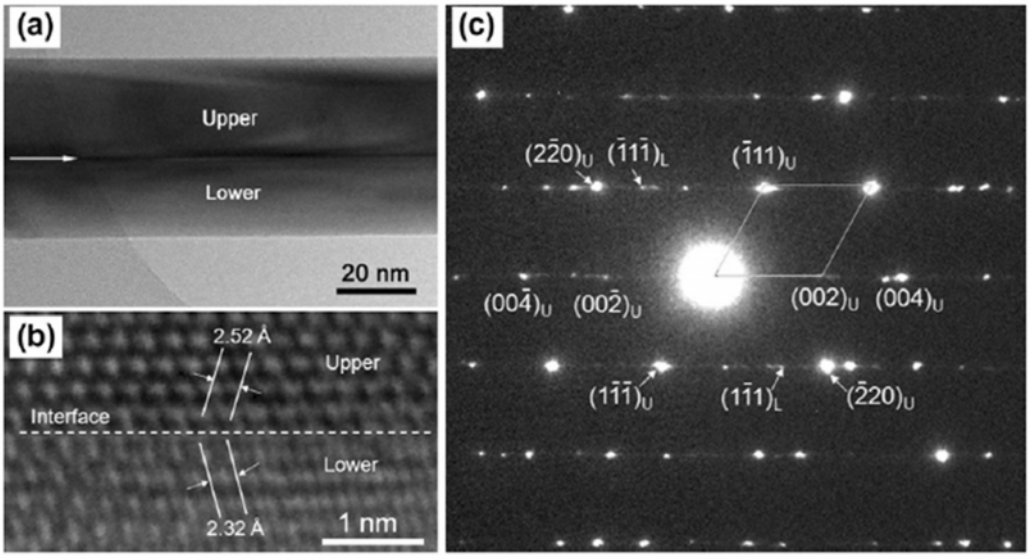

Figure 4: (a) The Contrast Feature from a BF TEM Image of an Individual CuO NW Suggests the Presence of a Twin Boundary Along the Axial Direction of the NW. (b) HRTEM Image of the NW Showing the Twin Boundary of the NW. (c) SAED Pattern Obtained from a Single NW. Indices with Subscript L refer to the Lower side of the NW Shown in (a and b); Indices with Subscript U Refer to the Upper Side [55]

By examining CuO NW growth during the oxidation of Cu, we have shown recently that the compressive stresses generated from the CuO/Cu_2O interfacial reaction serves as the driving force to stimulate CuO NW growth [55]. Since both Cu_2O and CuO are cation-deficient p-type oxides, it has been shown that the oxide growth is controlled by outward diffusion of cations during the oxidation of Cu, which suggests that the process should follow the parabolic growth law [37, 40, 56-60]. Our own measurements on the growth rates of the Cu_2O and CuO layers also confirm the parabolic growth behavior. The growth of Cu_2O layer requires decomposition of the oxygen-richer CuO layer to obtain the necessary oxygen. Due to their different molar volumes of Cu2O and CuO (the cell volumes of Cu_2O and CuO are 77.83 $Å^3$ and 81.16 $Å^3$, respectively), the local volume change will generate the stress at the CuO/Cu_2O interface region, which would serve as the driving force for outward diffusion of Cu atoms, in addition to the normal Cu cation diffusion flux driven by the chemical potential gradient established by the many-orders-of-magnitude difference in oxygen partial pressure between the oxide-atmosphere and oxide-metal interfaces. A schematic diagram of the NW growth mechanism is shown in Fig. 5a. The Cu ions are first delivered onto

the substrate surface via outward grain boundary diffusion driven by the interfacial stress. A fraction of the Cu ions are transferred onto the NW base by oxide surface diffusion and continue to diffuse from the NW base to the tip by NW surface diffusion. A quantitative kinetic model by correlating the oxide NW growth rates with the surface diffusion of Cu cations supplied from the underlying grain boundary diffusion is derived in our previous work, which shows good agreement with the experimental observations [38].

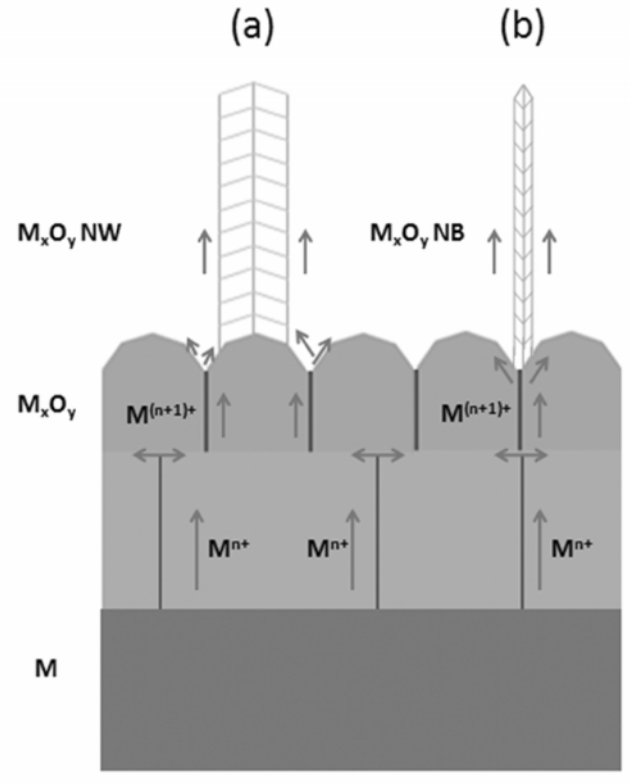

Figure 5: (a) Mass Transport Mechanisms of Metal ions for Metal Oxide NW Growth: Metal Ions Diffuse Outward from the Two Metal Oxides Interface to the Free Surface via GB Diffusion Driven by the Different Oxides Layers Interfacial Strain, Followed by Surface Diffusion from GB Junction Areas to the NW Root and then to the NW Tip Driven by the Concentration Gradient [55]. (b) Mass Transport Mechanisms of Metal Ions for the Growth of Metal Oxide Nanobelt [69]

3.2. Oxidation of Stressed Copper by Bending

To further confirm the stress effect on the CuO NW growth, the Cu foil is bent to apply stresses on the substrate, as shown in the middle of Fig. 6. As bending occurs, the compressive stress is generated in the upper surface, while the tension stress is in the bottom surface. After oxidation of the bent Cu foil, both the upper and bottom surfaces are covered with CuO NWs. Fig. 6 shows representative SEM images of the growth morphology of CuO NWs on the upper and bottom surfaces, respectively. It

can be seen that the density of NWs on the bottom surface of the bent Cu is much higher than the upper surface, suggesting evidently that in-plane tensile stresses result in significantly increased number density of CuO NWs as compared to the compressed Cu. Our cross-sectional SEM observations show that the formation of CuO NWs on all these Cu surfaces involves Cu_2O/CuO double layer growth with Cu_2O being the bottom layer and CuO being the top layer. Such a growth process imposes a correlation of the growth behaviors between the NWs and the oxide layers. Fig. 7 shows the cross sectional SEM images, which reveal that in the case of tensile stress the average sizes of Cu_2O and CuO grains are smaller than that of oxide grains affected by compressive stress. In addition, both the Cu_2O and CuO layers have larger thickness for the tensile stress case than that of the compressive stress [61].

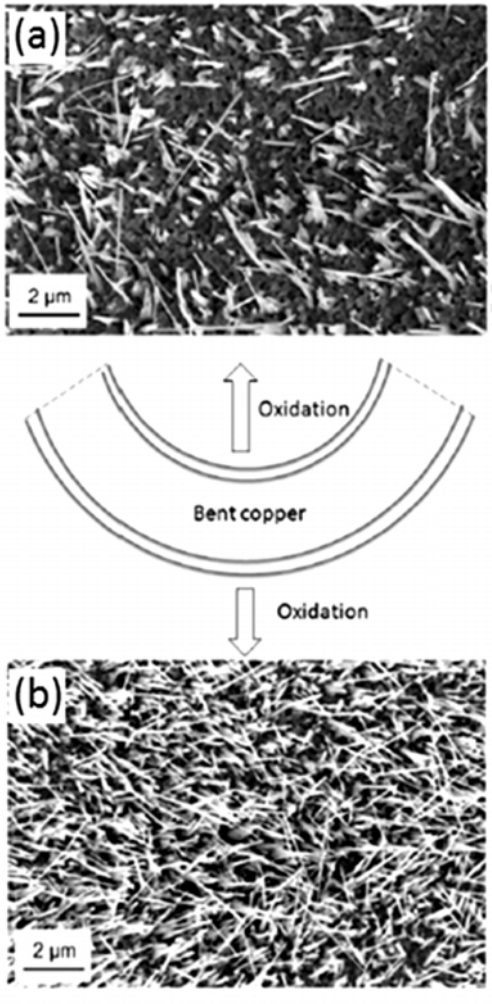

Figure 6: Schematic Diagram Showing the Generation of Stresses at the Upper and Bottom Surfaces of the Sample. SEM Images of the Oxide Surface for (a) Upper Surface of the Bent Cu and (b) Bottom Surface of the Bent Cu

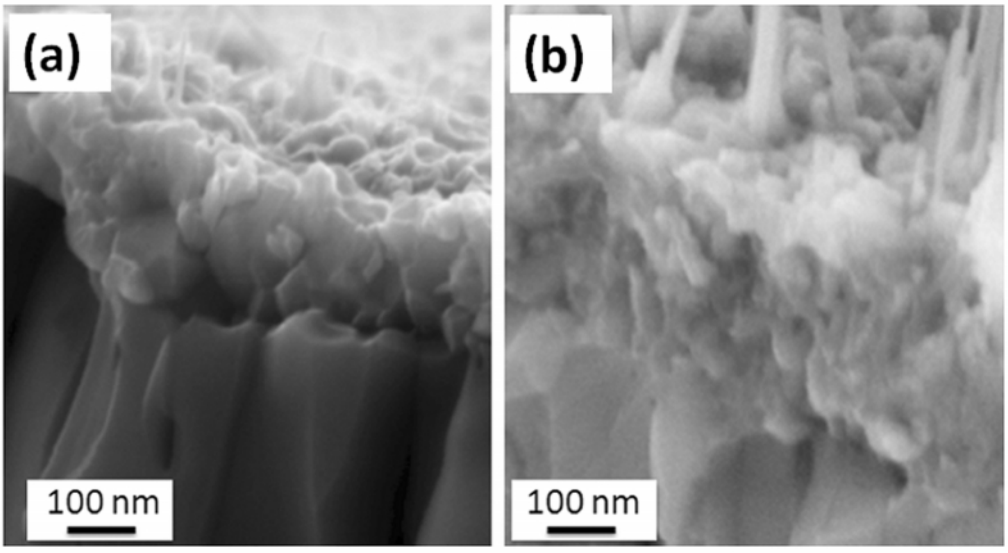

Figure 7: Cross-Sectional SEM Images of the Oxide Layers and Oxide Grain Morphologies for (a) Upper Surface of Bent Cu (Compressive Stress), and (b) Bottom Surface of Bent Cu (Tensile Stress) [61]

Based on the experimental observations and the NW growth mechanism discussed above, the effects of surface bending stresses on the oxide NW growth are schematically shown in Fig. 8 The tensile stresses on the substrate reduce the lattice mismatch strain between the inner layer of Cu_2O and the Cu substrate, which promotes the nucleation rate of Cu_2O islands and therefore increases the number of grain boundaries formed by impinged small Cu_2O grains. The increased grain boundaries enhance the efficient outward diffusion of Cu ions, which results in the increased growth of the thickness of the oxide layers and CuO NW length [61].

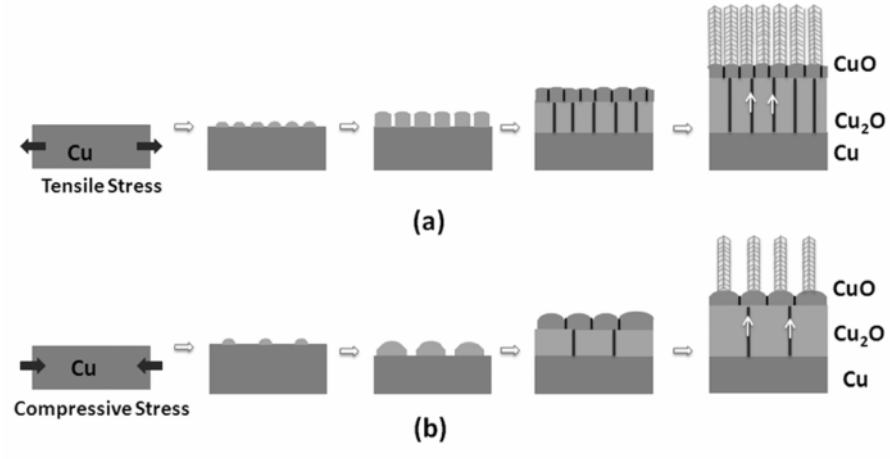

Figure 8: Schematic Showing the Effect of Surface Stresses on the Microstructure of the Oxide Layers and the Subsequent Oxide NW Growth, (a) Tensile Stress; (b) Compressive Stress [61]

3.3. Oxidation of Cu Surfaces Roughened by Sandblasting

Our results described above have shown that the oxide NW growth is closely related to the microstructures of the underlying oxide layers. Such a correlation is further verified by the oxidation of roughened Cu surfaces. By exerting sandblasting onto copper surfaces, we find that increasing the surface roughness can effectively promote CuO nanowire formation by significantly enhancing the NW growth density and length. Fig. 9 shows the evolution of the surface roughness of the copper substrates after being sandblasted with the different times. It can be seen that surface roughness increases with increasing the sandblasting time. Fig. 9(a) shows the optical profiler 3D surface morphology of the copper without being sandblasted, where the surface roughness is ~ 0.12 μm. Figs. 9(c) and (f) are 3D surface morphologies of the samples sandblasted for 3 s and 9 s, where the roughness is increased to 2.76 μm and 3.78 μm, respectively [62].

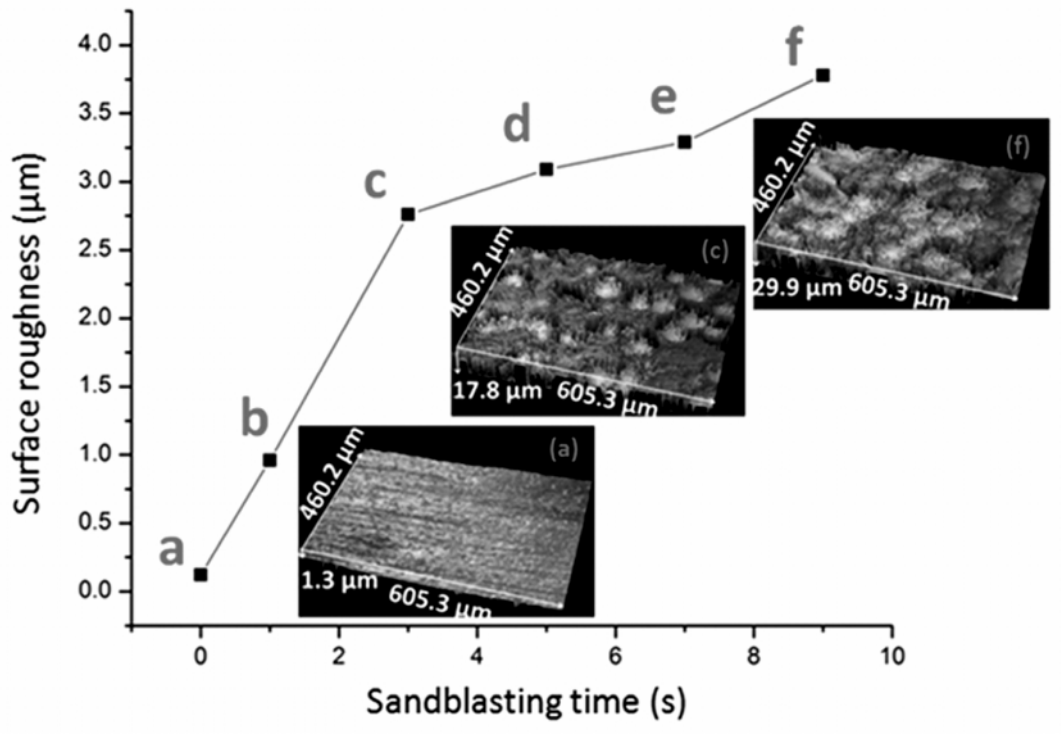

Figure 9: Surface Roughness of Cu Foils as a Function of the Sandblasting Time. (a), (c), (f) are 3D Surface Images Taken by Profilometer Showing the Surface Morphology of Samples Sandblasted for 0 s, 3 s, and 9 s, Respectively [62]

The sandblasted Cu foils are then oxidized simultaneously under the same conditions. It is observed that the increased surface roughness promote CuO NW formation in terms of both the density and growth length, as shown in Figs. 10(a, b, c). It also found that the increased surface roughness also results in the decreased grain

size and the increased thickness of CuO and Cu_2O, as shown in Figs. 10(d, e, f, g, h, i). Early-stage oxidation of copper investigated by in situ TEM reveals that the increased Cu surface roughness restricts the surface mobility of oxygen atoms [63-65], which gives rise to a higher nucleation density of Cu_2O islands and therefore Cu_2O grains are still small in their lateral size when they impinge with each other. The smaller gain size corresponds to a higher density of grain boundaries. The effectively increased fraction of grain boundaries is conducive to the outward diffusion of Cu ions to promote the layered oxide growth and CuO NW formation. This is because the CuO layer is formed on the Cu_2O inner layer, smaller Cu_2O grains results in finer CuO grains, which provide more surface sites for CuO NW nucleation to release the interfacial strain generated from the oxide-forming reaction at the CuO/Cu_2O interface [62]. Such an effect of the oxide microstructure on the oxide NW growth can be explained similarly using the schematic diagram of Fig. 8, where the increased surface roughness by sandblasting leads to enhanced nucleation of Cu_2O grains, an outcome similar as the effect of tensile stress.

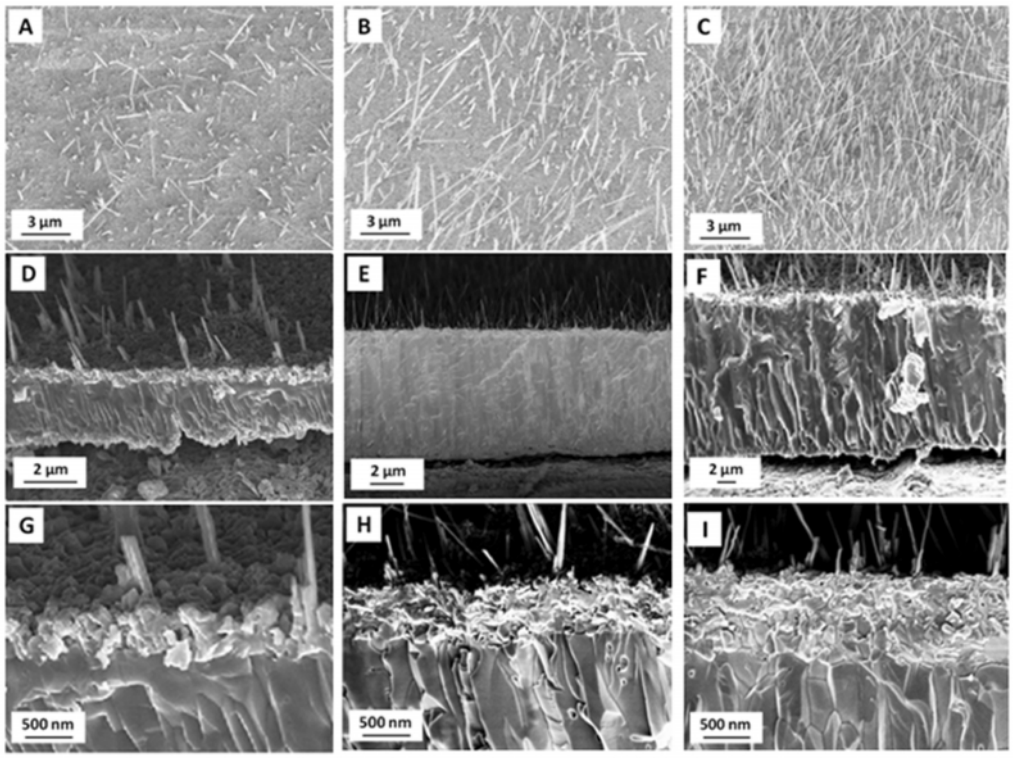

Figure 10: Top Surface (A, B, C) and Interface (D, E, F, G, H, I) SEM Images of Cu Substrates. A, D, G: the Surface Without Being Sandblasted; B, E, H: the Surface Sandblasted for 3 s; C, F, I: the Surface Sandblasted for 9 s. D, E, F are Low-Magnification SEM Images Showing the Overall Morphology of the Interfaces of Cu_2O/Cu and CuO/Cu_2O; and G, H, I are High-Magnification SEM Images from the CuO/Cu_2O Interface of the Three samples

4. GROWTH OF α-FE_2O_3 NWS DURING THE OXIDATION OF FE

To test if the oxide NW growth mechanism proposed above from the oxidation of Cu is applicable to other metal systems, our experimental system is extended to the oxidation of Fe. Fig. 11 are representative SEM images showing the growth of α-Fe_2O_3 NWs formed on Fe foils oxidized at 400°C and 600°C, respectively. The surfaces of both samples are covered by α-Fe_2O_3 NWs. At 400°C, the NW diameter is about 50 nm and lengths range from 100 nm to 2 m. At 600oC, the NWs diameters vary from 50 nm to 150 nm and the average length is about 5 m. Oxide NWs for both the oxidation temperatures have the tapered shape at the tip, as shown in the inset images in Fig. 11a and b. It also observed that the NW density, NW diameter and length all increase with the oxidation temperature. According to the iron-oxygen phase diagram, iron forms three thermodynamically stable oxides, FeO, Fe_3O_4 and Fe_2O_3 during oxidation process and the phase wustite (FeO) does not form below 570°C [66]. Therefore, the Fe foil oxidized below this temperature is expected to form a two-layer structure of Fe_3O_4 and Fe_2O_3 with the Fe_3O_4 next to the Fe substrate, as shown in Fig. 11c. Above 570°C, the oxide layer sequence in the scale is FeO, Fe_3O_4 and Fe_2O_3 , with the FeO layer next to Fe, as shown in Fig. 11d. From the results shown in Fig. 11, it can be seen that both the two-layer oxides structure and three-layer oxides structure can lead to the oxide NWs growth.

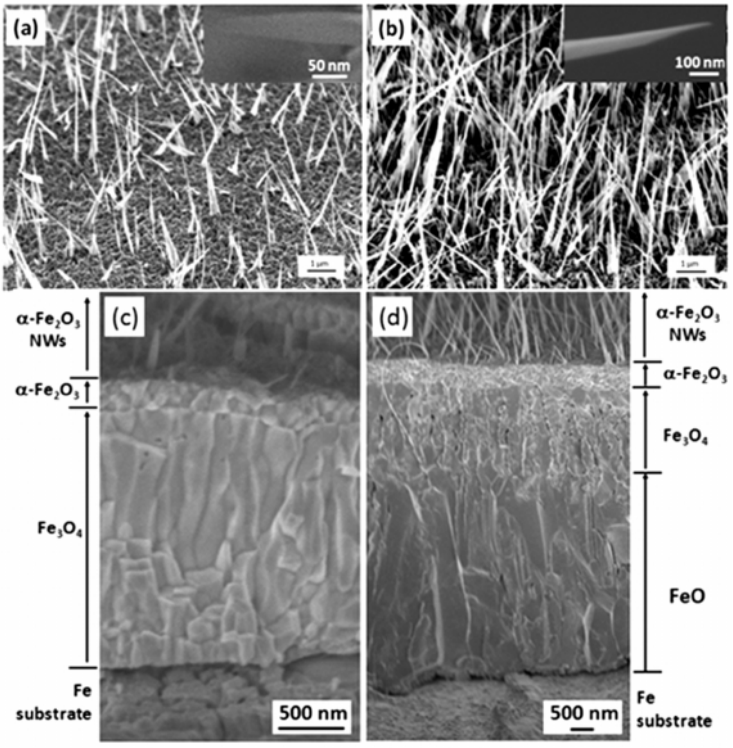

Figure 11: SEM Micrographs of the Surface and Interface Morphology of Fe Substrates Oxidized at (a, c) 400°C and (b, d) 600°C for 1h Under the Oxygen Pressure of 200 Torr

A typical bright-field (BF) TEM image of an individual α-Fe_2O_3 NW is shown in Fig. 12a. Fig. 12b shows two sets of the diffraction spots: one is along $(\bar{1}101)$ zone axis and the other has the [0001] zone axis. The diffraction pattern also reveals that the NW grows along the $(11\bar{2}0)$ direction. Fig. 12c displays a high-resolution TEM image from the NW, which shows clearly the presence of the twin boundary along the NW axial direction. Fourier transform patterns (Fig. 12d and e) from the two sides of the HRTEM image reveal that the left side of the NW is oriented along the Fe_2O_3 $(\bar{1}101)$ zone axis while the zone axis for the right side of the NW is along the direction Fe_2O_3[0001] [67].

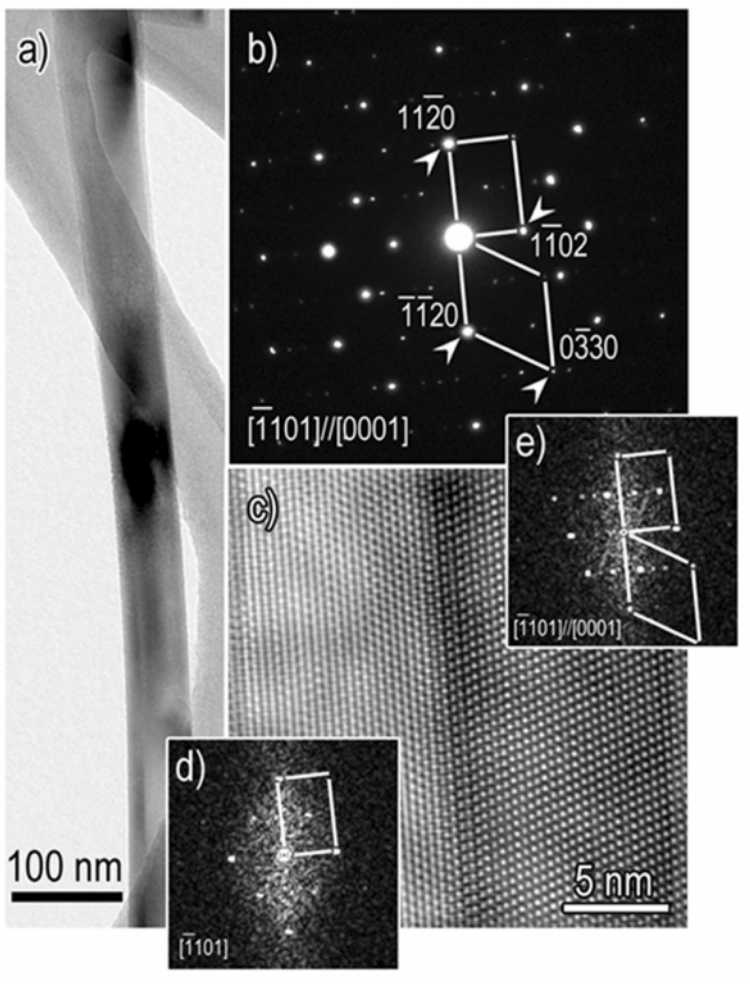

Figure 12: (a) BF TEM image of α-Fe_2O_3 NW. (b) SAED Obtained from the NW, Indexing of the Pattern Reveals Two Sets of Different Points with the Zone Axes of and [0001], Respectively. (c) HRTEM Image of the NW Confirms the Presence of the Twin Boundary. (d, e) Fourier Transform Patterns from Left and Right Side of the HRTEM Image [67]

The growth of α-Fe_2O_3 whiskers follows the same mechanism of CuO NWs formation. Fe_2O_3 NW growth is mainly associated with the stress generation and relaxation at the Fe_2O_3/Fe_3O_4 interface. Fe_3O_4 layer grows at the expense of the thin Fe_2O_3 layer at the Fe_2O_3/Fe_3O_4 interface. The Pilling and Bedworth's ratios (the ratio of the volume of the metal oxide to the volume of consumed metal) for FeO, Fe_3O_4, and Fe_2O_3, are 1.68, 2.10, and 2.14, respectively [68]. Since the specific volume of Fe_2O_3 is larger than that of Fe_3O_4, the compressive stresses are generated and accumulated in the bottom area of Fe_2O_3 layer, which will serve as the driving force for Fe_2O_3 NW growth.

5. TUNING THE GROWTH MORPHOLOGY OF 1D OXIDE NANOSTRUCTUTRES

Tailoring the morphology of nanostructures is one of the key challenges in the growth control. This is even more challenging for controlling the growth morphologies of oxide NWs during the oxidation, largely due to the convolution and coupling of different processes involved in the oxidation leading to the oxide NW formation, which includes layered oxide growth, interfacial reactions, mass transport, and stress generation and relaxation. Despite the complexity of the growth process, we show that it is still possible to tune the morphology of oxide NWs to some extent by controlling the sample preparation or oxidation conditions. Our experiments reveal that the growth of 1D α-Fe_2O_3 in the morphology of either nanowires or nanobelts (NBs) can be achieved by varying the oxygen gas pressure during the oxidation of Fe.

Figure 13 shows the SEM images of Fe foils oxidized for 1 hour at 600°C for the different oxygen gas pressures. The Fe surface is dominated by the growth of nanobelts with the width varying from 100 nm to 300 nm and length up to ~ 5 μm for oxygen pressures at 0.1 Torr. For the oxidation at 200 Torr, the oxidized surface is covered by a high density of nanowires with the diameter ranging from 50 to 150 nm and length up to 6 μm. The growth of the mixture of both nanowires and nanobelts occurs for the oxygen pressure between 0.1 Torr and 200 Torr. The side-view SEM images also reveal that both nanobelts and nanowires are perpendicular to the substrate surfaces at their roots. No significant differences in lengths are found for nanowires and nanobelts formed under the different oxygen gas pressures.

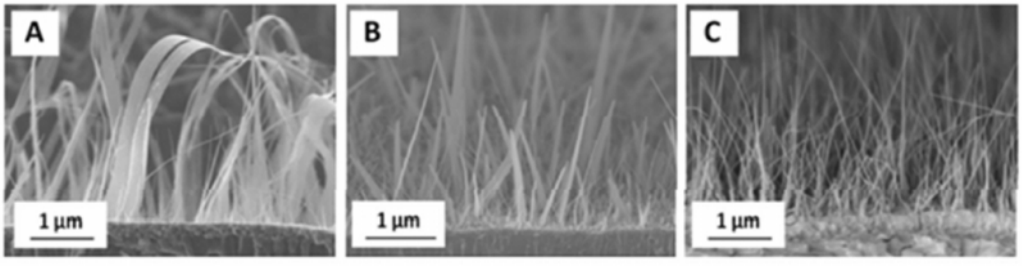

Figure 13: SEM Micrographs of the Surface Morphology of Fe Foils Oxidized at 600°C for 1h Under Different Oxygen Gas Pressures: (A) pO_2 = 0.1 Torr, (B) pO_2 = 50 Torr (B), and (C) pO_2 = 200 Torr

The microstrucutre of NBs is also examined by TEM. Fig. 14a shows a BF TEM image of a typical nanobelt with a width of ~ 200 nm. The selected area electron diffraction pattern obtained from the nanobelt is shown in Fig. 14b, which can be indexed with two sets of diffraction spots, one refers to an incident electron beam parallel to the [0001] zone axis and the other is the $(\bar{1}101)$ zone axis with $[0001]//[\bar{1}101]$. The appearance of the two sets of diffraction patterns from the same area suggests that the nanobelt has a bicrystal structure, similar as α-Fe_2O_3 NWs as shown in Fig. 12. From the morphology image and diffraction pattern, we can find that the length direction of the nanobelt is along $[11\bar{2}0]$. The HRTEM image of the nanobelt and the corresponding Fourier transform pattern shown in Fig. 14c further confirm the bicrystal structure of the nanobelt.

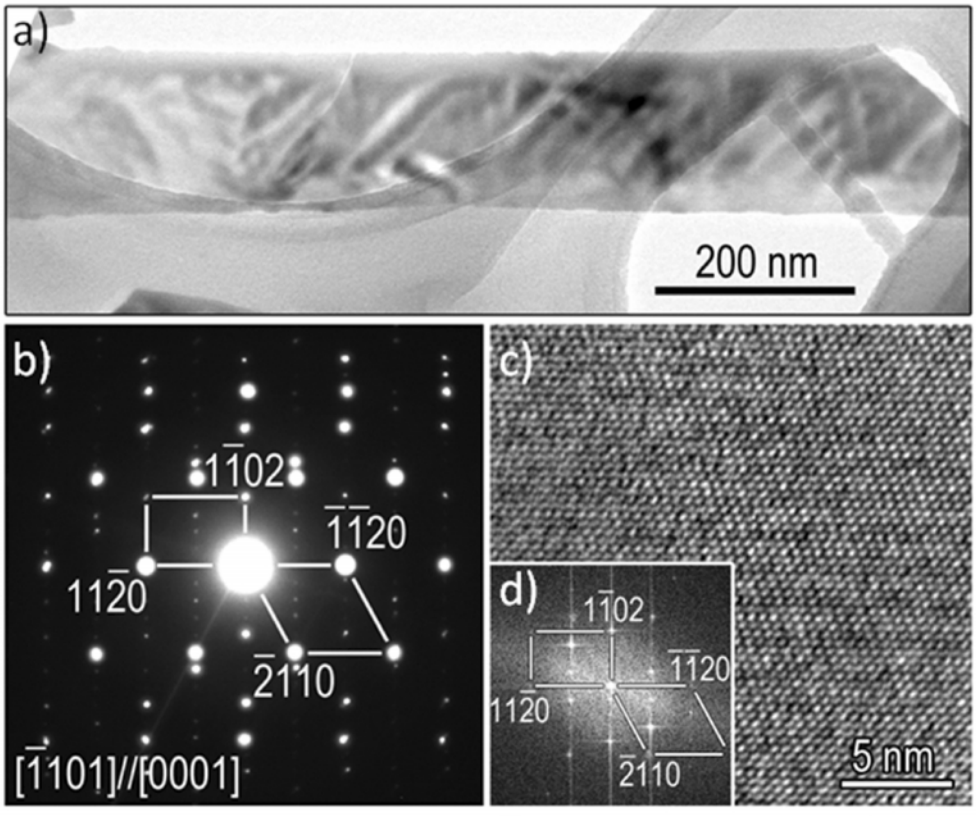

Figure 14: (a) Bright-Field (BF) TEM Image of an α-Fe_2O_3 Nanobelt Obtained from Oxidation at pO_2 = 0.1 Torr; (b) SAED Pattern from the Nanobelt in (a); (c) HRTEM Image of the Nanobelt in (a); (d) a Fourier Transform Pattern of the HRTEM [69]

The initial growth morphologies of the oxide NWs and NBs are examined by SEM. Figs. 15 (A, B) are SEM images showing the initially formed NWs and NBs on Fe substrates oxidized for only 30 min with pO_2 = 0.1 Torr and 10 min with pO_2 = 200 Torr, respectively. The SEM images reveal that both surfaces are covered with a layer

of α-Fe_2O_3 oxide grains for the two oxygen pressures and nanobelts and nanowires originate from different surface regions. It can be seen that nanobelts are associated with the grain boundary areas while nanowires are formed directly on top of grains. Side-view SEM images (Figs. 15C and D) obtained from the oxidized samples confirm these growth features. It becomes clear that NBs grow out of grain boundaries and the resulting morphology (wide in width but thin in thickness) is defined by the geometry of grain boundaries, i.e., wide and thin along the boundary, and nanowires grow on the top of grains and the resulting shape is correlated with the shape of grains.

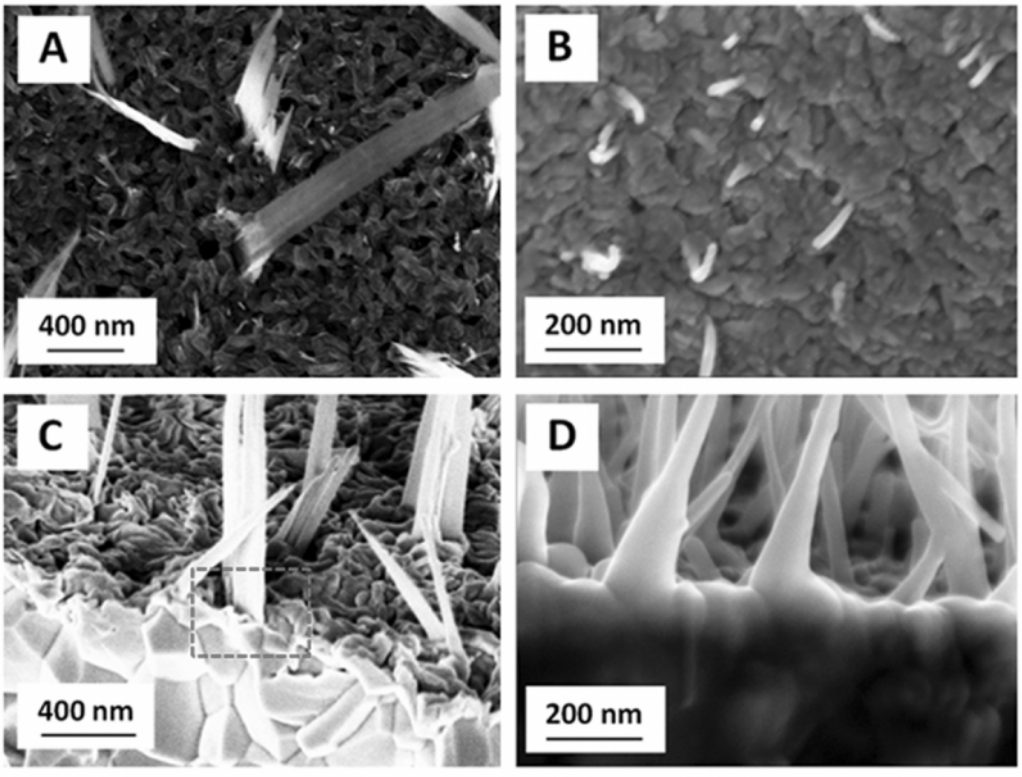

Figure 15: The Initial Growth Morphologies of Nanobelts and Nanowires: Upper Panel: Top Views of Fe foils Oxidized for 30 min at pO_2 = 0.1 Torr (A) and Oxidized for 10 min at pO_2 = 200 Torr (B); Lower Panel: Side-View SEM Micrographs showing the root regions of nanobelts and nanowires Obtained from the Oxygen Pressures of 0.1 Torr (C) and 200 Torr (D) [69]

Based on the above observations, the formation of α-Fe_2O_3 NB can be described as follows. With decreasing the oxygen gas pressure, the oxidation rate is slowed down and the Fe_3O_4/Fe_2O_3 interfacial reaction rate is thus reduced, which results in a smaller stress gradient across the Fe_2O_3 layer. Under the smaller driving force, Fe cations are delivered only onto the grain boundary region by grain boundary diffusion and deposit on the grain surfaces near the grain boundary nadir by reacting surrounding oxygen gas. The oxide nucleated on the surface of adjacent Fe_2O_3 grains grows and merges along the grain boundary, forming a bicrystal structure along the grain boundary with

the NB morphology which is correlated with the geometry of the grain boundary. However, if the oxygen gas pressure is large, the Fe_3O_4/Fe_2O_3 interfacial reaction is fast, which results in enhanced generation and accumulation of compressive stress at the Fe_3O_4/Fe_2O_3 interface. This leads to an increased stress gradient for Fe outward diffusion and promotes the delivery of Fe cations onto the top of Fe_2O_3 grains via combined grain boundary and surface diffusion, where grain surfaces serve as structure templates for the nucleation of Fe_2O_3 nanowires. Since grains typically show different surface facets, the crystal nucleated on the different facets of the grain grow and join each other at the grain top to form a bi-crystal or multi-crystal.

The comparison for the formation of NWs and NBs is schematically shown in Fig. 5. The formation of Fe_2O_3 NWs follows the same mechanism of CuO NWs, which is shown in Fig. 5a; while the growth mechanism of Fe_2O_3 NBs is shown in Fig. 5b. However, our experiments indicate that the growth of oxide NBs does not occur for the oxidation of Cu for different oxygen gas pressures. This difference in the growth morphologies of the 1D oxide nanostructures for the oxidation of Cu and Fe may be related to the different interfacial stresses. The Pilling and Bedworth's ratios for the formation of Cu_2O and CuO are 1.64 and 1.75 respectively, while the Pilling and Bedworth's ratios for the formation of Fe_3O_4 and Fe_2O_3 are 2.10, and 2.14, respectively. It is thus expected that the oxidation of Cu results in a larger interfacial strain generated at the Cu_2O/CuO interface than the Fe_3O_4/Fe_2O_3 interfacial strain for the oxidation of Fe due to the smaller molar volume difference between Fe_3O_4 and Fe_2O_3. Therefore, the larger stress gradient in the CuO layer facilitates the delivery of Cu cations onto the top of CuO grains, resulting in CuO nanowire growth during the oxidation of Cu, while for the oxidation of Fe under the relatively low oxygen gas pressure, Fe cations may be delivered only onto the grain boundary area due to the smaller stress gradient in the Fe_2O_3 layer, resulting in the growth of Fe_2O_3 NBs.

6. SUMMARY

We systematically investigated 1D oxide growth during the oxidation of Cu and Fe. The occurrence of oxide NWs is identified by atom diffusion rather than mechanical flow. The interfacial strain associated with the oxide-forming interfacial reaction during the layered oxide growth drives outward grain-boundary diffusion of cations, which acts as a continual source of metal ions for oxide NW growth at the tip. By exerting bending stresses on Cu surfaces, we show that in-plane tensile stresses can effectively promote CuO NW formation by significantly increasing the NW growth density. By applying sandblasting onto copper surfaces, we find that increasing the surface roughness can effectively promote CuO nanowire formation by significantly enhancing the nanowire growth density and length during the oxidation of Cu. These results demonstrate that both in-plane tensile stresses and surface roughening can lead to finer grain structures in the layered oxide growth, thereby facilitating outward diffusion of Cu ions for enhanced oxide NW growth. Extension of the study to the oxidation of Fe demonstrates a greater universality of the principle of stress-driven oxide NW formation during the oxidation of metals. Although the oxidation of both Cu and Fe

can form oxide nanowires under certain thermal oxidation conditions and follow the similar growth mechanism, they also have some differences during the oxidation process. The oxidation of Cu forms two oxide layers (CuO and Cu_2O) during oxidation; while the oxidation of Fe can form either two oxide layers (α-Fe_2O_3 and Fe_3O_4) or three oxide layers (α-Fe_2O_3, Fe_3O_4 and FeO) depending on the oxidation conditions. Moreover, the oxidation of Cu forms CuO NWs only; while the oxidation of Fe can form Fe_2O_3 NWs and NBs of 1D by changing the oxygen gas pressure. These differences can be attributed to their different interfacial strains that depend on the molar volumes between the layered oxides. It is found that the interfacial strain at the Fe_2O_3/Fe_3O_4 interface can be enhanced by increasing the oxygen gas pressure, resulting in a transition from the growth of Fe_2O_3 NBs to Fe_2O_3 NWs.

ACKNOWLEDGEMENTS

This work was supported by National Science Foundation Grant No. CMMI-0825737. The authors would like to thank Rediola Mema, Yiqian Wang, Jianbo Wang, Qike Jiang, Rongsheng Cai, and Qingtian Du for help with the experiments.

REFERENCE

[1] E. Comini, C. Baratto, G. Faglia, M. Ferroni, A. Vomiero, and G. Sberveglieri, "Quasi-One Dimensional Metal Oxide Semiconductors: Preparation, Characterization and Application as Chemical Sensors", *Progress in Materials Science*, **54,** pp. 1-67, 2009.

[2] J. G. Lu, P. Chang, and Z. Fan, "Quasi-One-Dimensional Metal Oxide Materials-Synthesis, Properties and Applications", *Materials Science and Engineering: R: Reports*, **52,** pp. 49-91, 2006.

[3] Z. L. Wang, "Characterizing the structure and properties of Individual Wire-Like Nanoentities", *Adv Materials*, **12,** pp. 1295, 2000.

[4] A. Kolmakov and M. Moskovits, "Chemical Sensing and Catalysis by One-Dimensional Metal-Oxide Nanostructures", *Annual Review of Materials Research*, **34,** pp. 151-180, 2004.

[5] N. D. Cuong, Y. W. Park, and S. G. Yoon, "Microstructural and Electrical Properties of Ga2O3 Nanowires Grown at Various Temperatures by Vapor-Liquid-Solid Technique", *Sensors and Actuators B: Chemical*, **140,** pp. 240-244, 2009.

[6] Y. L. Chueh, M. W. Lai, J. Q. Liang, L. J. Chou, and Z. L. Wang, "Systematic Study of the Growth of Aligned Arrays of α-Fe_2O_3 and Fe_3O_4 Nanowires by a Vapor-Solid Process", Advanced Functional Materials, 16, pp. 2243-2251, 2006.

[7] X. Zhang, X. Shan, J. Zhang, L. Chen, J. Xu, L. You, and D. Yu, "In Situ Study of Epitaxial Growth of ZnO Nanowires at The Junctions of Nanowall Networks on Zinc Particles", *Micron*, **40,** pp. 302-7, Apr 2009.

[8] C. Xu, K. Hong, S. Liu, G.wang, and X. Zhao, "A Novel Wet Chemical Route to NiO Nanowires", *Journal of Crystal Growth*, **255,** pp. 308-312, 2003.

[9] A. Mahapatra, B. G. Mishra, and G. Hota, "Synthesis of Ultra-Fine α-Al_2O_3 Fibers Via Electrospinning Method", *Ceramics International*, **37,** pp. 2329-2333, 2011.

[10] Seu Yi Li, Chia Ying Lee, and T. Y. Tseng, "Copper-Catalyzed ZnO Nanowires On Silicon (1 0 0) Grown By Vapor-Liquid-Solid Process", *Journal of Crystal Growth*, **247,** 2003.

[11] W. Zheng, D. Sheng, and H. Douglas, "Gallium-Catalyzed Silicon Oxide Nanowire Growth", *Tsinghua Science & Technology*, **10,** pp. 718-728, 2005.

[12] I. Castro-hurtado, J. Herrán, G. Ga Mandayo, and E. Castaño, "SnO_2 Nanowires Grown by Catalytic Oxidation of Tin Sputtered thin Films for Formaldehyde Detection", Thin Solid Films, 2011.

[13] A. Vomiero, S. Bianchi, E. Comini, G. Faglia, M. Ferroni, and G. Sberveglieri, "Controlled Growth and Sensing Properties of In_2O_3 Nanowires", *Crystal Growth and Design*, **7,** pp. 2500-2504, 2007.

[14] J. Lee, M. Islam, and S. Kim, "Photoresponses of ZnO Nanobridge Devices Fabricated Using a Single-Step Thermal Evaporation Method", *Sensors and Actuators B: Chemical*, **126,** pp. 73-77, 2007.

[15] Y. Wang, J. Xu, R. Wang, and D. Yu, "Electron Microscopy Investigation of Gallium Oxide Micro/Nanowire Structures Synthesized Via Vapor Phase Growth", *Micron*, 35, pp. 447-453, 2004.

[16] B. Kang, Y. Heo, L. Tien, D. Norton, F. Ren, B. Gila, and S. Pearton, "Hydrogen and Ozone Gas Sensing Using Multiple ZnO Nanorods", *Applied Physics A: Materials Science & Processing*, **80,** pp. 1029-1032, 2005.

[17] K. Goodman, V. Protasenko, J. Verma, T. Kosel, G. Xing, and D. Jena, "Molecular Beam Epitaxial Growth of Gallium Nitride Nanowires on Atomic Layer Deposited Aluminum Oxide", *Journal of Crystal Growth*, **334**, pp. 113-117, 2011.

[18] G. Mor, O. K. Varghese, M. Paulose, N. Mukherjee, and C. Grimes, "Fabrication of Tapered, Conical-Shaped Titania Nanotubes", *Journal of Materials Research*, **18,** pp. 2588-2593, 2003.

[19] Y. Tan, X. Xue, Q. Peng, H. Zhao, T. Wang, and Y. Li, "Controllable Fabrication and Electrical Performance of Single Crystalline Cu_2O Nanowires with High Aspect Ratios", *Nano Letters*, **7,** pp. 3723-3728, 2007.

[20] Y. Shin, M. Hohman, M. Brenner, and G. Rutledge, "Experimental Characterization of Electrospinning: the Electrically Forced Jet and Instabilities", *Polymer*, **42,** pp. 09955-09967, 2001.

[21] W. Y. Wu, J. M. Ting, and P. J. Huang, "Electrospun ZnO Nanowires as Gas Sensors for Ethanol Detection", *Nanoscale Research Letters*, **4,** pp. 513-517, 2009.

[22] X. Lu, X. Liu, W. Zhang, C. Wang, and Y. Wei, "Large-Scale Synthesis of Tungsten Oxide Nanofibers by Electrospinning", *Journal of Colloid and Interface Science*, **298,** pp. 996-999, 2006.

[23] H. Guan, C. Shao, S. Wen, B. Chen, J. Gong, and X. Yang, "Preparation and Characterization of NiO Nanofibres Via an Electrospinning Technique", *Inorganic Chemistry Communications*, **6,** pp. 1302-1303, 2003.

[24] H. Dai, J. Gong, H. Kim, and D. Lee, "A Novel Method for Preparing Ultra-Fine Alumina-Borate Oxide Fibres via an Electrospinning Technique", *Nanotechnology*, **13,** pp. 674, 2002.

[25] R. Takagi, "Growth of oxide whiskers on metals at high temperature," J. Phys. Soc. Japan, vol. 12, pp. 1212-1218, 1957.

[26] X. C. Jiang, T. Herricks, and Y. N. Xia, "CuO Nanowires can be Synthesized by Heating Copper Substrates in Air", *Nano Letters*, **2,** pp. 1333-1338, 2002.

[27] A. M. Goncalves, L. C. Campos, A. S. Ferlauto, and R. G. Lacerda, "On the Growth and Electrical Characterization of CuO Nanowires by Thermal Oxidation", *Journal of Applied Physics*, **106,** pp. 034303, 2009.

[28] I. Avramov, "Kinetics of Growth of Nanowhiskers (Nanowires and Nanotubes)", *Nanoscale Res Lett*, **2,** pp. 235-9, 2007.

[29] X. Jiang, T. Herricks, and Y. Xia, "CuO Nanowires Can Be Synthesized by Heating Copper Substrates in Air", *Nano Letters*, **2,** pp. 1333-1338, 2002.

[30] H. Siegbahn, L. Asplund, P. Kelfve, K. Hamrin, L. Karlsson, and K. Siegbahn, "ESCA Applied to Liquids. II. Valence and Core Electron Spectra of Formamide", *Journal of Electron Spectroscopy and Related Phenomena*, **5,** pp. 1059-1079, 1976.

[31] B. J. Hansen, H.-l. Chan, J. Lu, G. Lu, and J. Chen, "Short-Circuit Diffusion Growth of Long bi-Crystal CuO Nanowires", *Chemical Physics Letters*, **504,** pp. 41-45, 2011.

[32] J. T. Chen, F. Zhang, J. Wang, G. A. Zhang, B. B. Miao, X. Y. Fan, D. Yan, and P. X. Yan, "CuO Nanowires Synthesized by Thermal Oxidation route", *Journal of Alloys and Compounds*, **454,** pp. 268-273, 2008.

[33] C. Geng, Y. Jiang, Y. Yao, X. Meng, J. A. Zapien, C. S. Lee, Y. Lifshitz, and S. T. Lee, "Well?Aligned ZnO Nanowire Arrays Fabricated on Silicon Substrates", *Advanced Functional Materials*, **14,** pp. 589-594, 2004.

[34] L. Huang, "Preparation of Large-Scale Cupric Oxide Nanowires by Thermal Evaporation Method", *Journal of Crystal Growth*, **260,** pp. 130-135, 2004.

[35] M. L. Zhong, D. C. Zeng, Z. W. Liu, H. Y. Yu, X. C. Zhong, and W. Q. Qiu, "Synthesis, Growth Mechanism and Gas-sensing Properties of Large-Scale CuO Nanowires", *Acta Materialia*, **58,** pp. 5926-5932, 2010.

[36] F. García-Labiano, L. F. De Diego, J. Adánez, A. Abad, and P. Gayán, "Temperature Variations in the Oxygen Carrier Particles During Their Reduction and Oxidation in a Chemical-Looping Combustion System", *Chemical Engineering Science*, **60,** pp. 851-862, 2005.

[37] G. M. Raynaud and R. A. Rapp, "In Situ Observation of Whiskers, Pyramids and Pits During the High-Temperature Oxidation of Metals", *Oxidation of Metals*, **21,** pp. 89-102, 1984.

[38] M. Komatsu and H. Mori, "In situ HVEM Study on Copper Oxidation Using an Improved Environmental Cell", *Journal of Electron Microscopy*, **54,** pp. 99-107, 2005.

[39] P. Kofstad, High temperature corrosion. New York: Elsevier Applied Science, 1988.

[40] R. A. Rapp, "The High Temperature Oxidatoin of Metals Forming Cation-Diffusing Scales", *Metallurgical Transactions B*, **15**B, pp. 195-212, 1983.

[41] D. A. Voss, E. P. Bulter, and T. E. Michell, "The Growth of Hermatite Blades During the High Temperature Oxidation of Iron", *Metallurgical Transactions A*, **13**A, pp. 929, 1982.

[42] M. Kaur, K. P. Muthe, S. K. Despande, S. Choudhury, J. B. Singh, N. Verma, S. K. Gupta, and J. V. Yakhmi, "Growth and Branching of CuO Nanowires by Thermal Oxidation of Copper", *Journal of Crystal Growth*, **289,** pp. 670-675, 2006.

[43] A. Kumar, A. K. Srivastava, P. Tiwari, and R. V. Nandedkar, "The Effect of Growth Parameters on the Aspect Ratio and Number Density of CuO Nanorods", *Journal of Physics: Condensed Matter*, **16,** pp. 8531-8543, 2004.

[44] L. Liao, Z. Zhang, B. Yan, Z. Zheng, Q. L. Bao, T. Wu, C. M. Li, Z. X. Shen, J. X. Zhang, H. Gong, J. C. Li, and T. Yu, "Multifunctional CuO Nanowire Devices: p-Type Field Effect Transistors and CO Gas Sensors", *Nanotechnology,* **20,** p. 085203, 2009.

[45] S. C. Vanithakumari, S. L. Shinde, and K. K. Nanda, "Controlled Synthesis of CuO Nanostructures on Cu Foil, Rod and Grid", *Materials Science and Engineering*: B, **176,** pp. 669-678, 2011.

[46] X. Wen, S. Wang, Y. Ding, Z. L. Wang, and S. Yang, "Controlled Growth of Large-Area, Uniform, Vertically Aligned Arrays of r-Fe_2O_3 nanobelts and nanowires", *J. Phys. Chem. B*, pp. 215-220, 2005.

[47] K. Zhang, C. Rossi, C. Tenailleau, P. Alphonse, and J.-Y. Chane-Ching, "Synthesis of Large-Area and Aligned Copper Oxide Nanowires from Copper thin Film on Silicon Substrate", *Nanotechnology*, **18,** pp. 275607, 2007.

[48] C. H. Xu, C. H. Woo, and S. Q. Shi, "Formation of CuO Nanowires on Cu Foil", *Chemical Physics Letters*, **399,** pp. 62-66, 2004.

[49] A. G. Nasibulin, S. Rackauskas, H. Jiang, Y. Tian, P. R. Mudimela, S. D. Shandakov, L. I. Nasibulina, S. Jani, and E. I. Kauppinen, "Simple and Rapid Synthesis of α-Fe_2O_3 Nanowires Under Ambient Conditions", *Nano Research*, 2, pp. 373-379, 2010.

[50] P. Hiralal, S. Saremi-Yarahmadi, B. C. Bayer, H. Wang, S. Hofmann, K. G. Upul Wijayantha, and G. A. J. Amaratunga, "Nanostructured Hematite Photoelectrochemical Electrodes Prepared by the Low Temperature Thermal Oxidation of Iron", *Solar Energy Materials and Solar Cells*, **95,** pp. 1819-1825, 2011.

[51] J. Chen, L. Xu, W. Li, and X. Gou, "α-Fe_2O_3 Nanotubes in Gas Sensor and Lithium-Ion Battery Applications", *Adv. Mater.*, **17,** pp. 582-586, 2005.

[52] S. Q. Liu and K. L. Huang, Sol. Energy Mater. Sol. Cells, **85,** pp. 125-131, 2005.

[53] T. Tepper, F. Ilievski, C. A. Ross, T. R. Zaman, R. J. Ram, S. Y. Yung, and B. Stadler, *J. Appl. Phys.*, **93,** pp. 6948, 2003.

[54] M. W. Barsoun, E. N. Hoffman, R. D. Doherty, S. Gupta, and A. Zavaliangos, "Driving Force and Mechanism for Spontaneous Metal Whisker Formation", *Phys. Rev. Lett.*, **93,** pp. 206-104, 2004.

[55] L. Yuan, Y.Q. Wang, R. Mema, and G. W. Zhou, "Driving Force and Growth Mechanism for Spontaneous Oxide Nanowire Formation During the Thermal Oxidation of Metals", *Acta Materialia*, **59,** pp. 2491-2500, 2011.

[56] H. E. Evans, "Stress Effects in High Temperature Oxidation of Metals", *International Journal of Materials Research*, **40,** pp. 1-40, 1995.

[57] Y. Zhu, K. Mimura, and M. Isshiki, "Oxidation Mechanism of Cu_2O to CuO at 600-1050°C", *Oxidation of Metals*, **62,** pp. 207-222, 2004.

[58] Y. F. Zhu, K. Mimura, and M. Isshiki, "Oxidation Mechanism of Copper at 623-1073K", *Materials Transactions*, **43,** pp. 2173-2176, 2002.

[59] Z. Grzesik and M. Migdalska, "On the Mechanism of Cu_2O Oxidation at High Temperature", *Defect and Diffusion Forum*, 289-292, pp. 429-436, 2009.

[60] Y. F. Zhu, K. Mimura, J. W. Lim, M. Isshiki, and Q. Jiang, "Brief Review of Oxidation Kinetics of Copper at 350°C to 1050°C", *Metalluraical and Materials Transactions A*, **37**A, pp. 1231-1237, 2006.

[61] R. Mema, L. Yuan, Q. T. Du, Y. Q. Wang, and G. W. Zhou, "Effect of Surface Stresses on CuO Nanowire Growth in the Thermal Oxidation of Copper", *Chemical Physics Letters*, **512,** pp. 87-91, 2011.

[62] L. Yuan and G. W. Zhou, "Enhanced CuO Nanowire Formation by Thermal Oxidation of Roughened Copper", *Journal of The Electrochemical Society*, **159,** pp. C1, 2012.

[63] J. C. Yang, M. Yeadon, B. Kolasa, and J. M. Gibson, "Oxygen Surface Diffusion in Three-Dimensional CuO Growth on Cu (001) Thin Films", *Applied Physics Letters*, **70,** pp. 3522, 1997.

[64] J. C. Yang, M. Yeadon, B. Kolasa, and J. M. Gibson, "The Homogeneous Nucleation Mechanism of Cu_2O on Cu(001)", *Scripta Materialia*, **38,** pp. 1237-1242, 1998.

[65] G. W. Zhou, J. C. Yang, "Initial Oxidation Kinetics of Copper (110) Film Investigated by in Situ UHV-TEM", *Surface Science*, **531,** pp. 359-367, 2003.

[66] N. Birks, G. H. Meier, and F. S. Pettit, Introduction to the High Temperature Oxidation of Metals, 2nd ed. Cambridge: Cambridge University Press, 2006.

[67] L. Yuan, Y. Wang, R. Cai, Q. Jiang, J. Wang, B. Li, A. Sharma, and G. Zhou, "The Origin of Hematite Nanowire Growth During the Thermal Oxidation of Iron", *Materials Science and Engineering*: B, **177** pp. 327-336, 2012.

[68] M. Schutze, Protective Oxide Scales and their Breakdown. West Sussex, England: John Wiley and Sons, 1997.

[69] Lu Yuan, Qike Jiang, Jianbo Wang, and G. Zhou, "The Growth of Hematite Nanobelts and Nanowires - Tune the Shape Via Oxygen Gas Pressure", *Journal of Materials Research*, p. In press, April 14 2012.